NeuroImage xxx (2012) xxx–xxx

Contents lists available at SciVerse ScienceDirect

NeuroImage

journal homepage: www.elsevier.com/locate/ynimg

Brain maturation: Predicting individual *BrainAGE* in children and adolescents using structural MRI

Katja Franke [a,*], Eileen Luders [b], Arne May [c], Marko Wilke [d,f,g], Christian Gaser [a,e]

[a] Department of Psychiatry, Jena University Hospital, 07743 Jena, Germany
[b] Laboratory of Neuro Imaging, Department of Neurology, UCLA School of Medicine, Los Angeles, CA 90095-7334, USA
[c] Department of Systems Neuroscience, University of Hamburg, 22046 Hamburg, Germany
[d] Paediatric Neurology & Developmental Medicine, Children's Hospital, 72076 Tübingen, Germany
[e] Department of Neurology, Jena University Hospital, 07743 Jena, Germany
[f] Experimental Pediatric Neuroimaging, Children's Hospital, 72076 Tübingen, Germany
[g] Department of Neuroradiology, University Hospital, 72076 Tübingen, Germany

ARTICLE INFO

Article history:
Accepted 2 August 2012
Available online xxxx

Keywords:
BrainAGE
Prediction
Brain maturation
Gray matter
White matter
Structural MRI
Developmental delay

ABSTRACT

Background: Neural development during human childhood and adolescence involves highly coordinated and sequenced events, characterized by both progressive and regressive processes. Despite a multitude of results demonstrating the age-dependent development of gray matter, white matter, and total brain volume, a reference curve allowing prediction of structural brain maturation is still lacking but would be clinically valuable. For the first time, the present study provides a validated reference curve for structural brain maturation during childhood and adolescence, based on structural MRI data.

Methods and findings: By employing kernel regression methods, a novel but well-validated *BrainAGE* framework uses the complex multidimensional maturation pattern across the whole brain to estimate an individual's brain age. The *BrainAGE* framework was applied to a large human sample (n = 394) of healthy children and adolescents, whose image data had been acquired during the NIH MRI study of normal brain development. Using this approach, we were able to predict individual brain maturation with a clinically meaningful accuracy: the correlation between predicted brain age and chronological age resulted in r = 0.93. The mean absolute error was only 1.1 years. Moreover, the predicted brain age reliably differentiated between all age groups (i.e., preschool childhood, late childhood, early adolescence, middle adolescence, late adolescence). Applying the framework to preterm-born adolescents resulted in a significantly lower estimated brain age than chronological age in subjects who were born before the end of the 27th week of gestation, demonstrating the successful clinical application and future potential of this method.

Conclusions: Consequently, in the future this novel *BrainAGE* approach may prove clinically valuable in detecting both normal and abnormal brain maturation, providing important prognostic information.

Introduction

Human brain development involves highly coordinated and sequenced events characterized by both progressive (e.g., cell growth and myelination) and regressive (e.g., synaptic pruning) processes (Silk and Wood, 2011). Especially with the advent of magnetic resonance imaging (MRI), cross-sectional as well as longitudinal neuroimaging studies contributed to a better understanding of healthy brain maturation. In addition, with the availability of automated computational methods for analyzing MRI data, such as voxel-based morphometry (VBM; Ashburner and Friston, 2000), it has become feasible to quantify and visualize structural brain changes in vivo (May, 2011) in truly healthy children, which effectively was not possible before (Giedd et al., 1996).

Volumetric MRI studies have reliably established the overall pattern of an initial rapid increase in total gray matter (GM) volume, followed by a phase of slower growth and, after reaching a peak in childhood, by a slow but continued reduction. In contrast, total white matter (WM) volume increases rapidly until the age of 10–15 years, with continued gain well beyond adolescence (Giedd et al., 1999; Groeschel et al., 2010; Silk and Wood, 2011). With the growing number of studies that have investigated both normal and abnormal brain changes with age, most major neuropsychiatric disorders are now thought to arise due to deviations from normal brain development during childhood and/or adolescence (Giedd et al., 2009; Paus et al., 2008). For some of these (e.g., childhood-onset schizophrenia or pediatric bipolar disorder),

* Corresponding author at: Structural Brain Mapping Group, Department of Psychiatry, Jena University Hospital, Jahnstr. 3, D-07743 Jena, Germany. Fax: +49 3641 934755.
E-mail addresses: katja.franke@uni-jena.de (K. Franke), eileen@loni.ucla.edu (E. Luders), a.may@uke.uni-hamburg.de (A. May), marko.wilke@med.uni-tuebingen.de (M. Wilke), christian.gaser@uni-jena.de (C. Gaser).

1053-8119/$ – see front matter © 2012 Published by Elsevier Inc.
http://dx.doi.org/10.1016/j.neuroimage.2012.08.001

early detection afforded by a brain maturation reference curve would be clinically relevant.

Recently, Dosenbach et al. (2010) emphasized the need of maturation curves for pediatric brain development to aid in the early detection of neurodevelopmental disorders. They reported how brain maturity across development can be predicted with functional connectivity MRI (fcMRI). Using fcMRI data of 238 healthy subjects (aged 7 to 30 years), they predicted a maturation curve that accounted for 55% of the sample variance. Given the clinical potential of such predictions, approaches that lead to accounted variances of even more than 55% would be highly attractive. At the same time, it would be desirable to keep the duration of image acquisition as short as possible due to the known difficulties of motion artifacts in pediatric MRI studies (Wilke et al., 2008; Yuan et al., 2009). Moreover, such approaches will maintain a high impact on clinical diagnosis and intervention only if they are less prone to measurement bias due to individual alertness and vigilance (Van Dijk et al., 2012).

Focusing on these facts, our group has recently developed a new approach based on structural MRI data that enables one to reliably estimate the brain age of any given subject (Franke et al., 2010). By employing kernel regression methods in a large training database, the complex multidimensional aging patterns across the whole brain are detected and aggregated to one single value (i.e., the estimated brain age). Consequently, although using only one MRI scan per subject, the degree of acceleration or deceleration of brain aging can be directly quantified in terms of years allowing a wide range of analyses and predictions on an individual level. In an exemplary analysis with elderly adults, this brain age estimation model showed its potential to provide clinically relevant information by reporting a statistically significant, positive deviation of 10 years between the estimated and chronological ages in patients with Alzheimer's disease, indicating accelerated brain atrophy and underlining the diagnostic potential of such an approach.

In the present study we show the potential of our *BrainAGE* framework to reliably predict structural maturity levels of brains from healthy children and adolescents ranging between 5 and 18 years based on one structural MR scan per subject. Further, the age estimation framework will be exemplarily applied to a clinical sample of adolescents born preterm. We hypothesize that the group with a very low gestational age (GA<27 weeks) would have a significantly lower estimated brain age than the group with a higher gestational age (GA>29 weeks) due to decelerated brain maturation, which is presumed to be caused by the extremely premature birth status.

Methods

Subjects/database

Data used in the preparation of this article were obtained from the Pediatric MRI Data Repository created by the NIH MRI Study of Normal Brain Development. This multisite study of typically developing children and adolescents was conducted by the National Institute of Child Health and Human Development, the National Institute on Drug Abuse, the National Institute of Mental Health, and the National Institute of Neurological Disorders and Stroke (Evans, 2006). We used structural MRI data from objective 1, which included 432 healthy children and adolescents of either sex aged 5–18 years (one T1-weighted image per subject). As data quality interfered with data processing (see Image processing), the data of a total of 38 subjects was excluded, leaving a final sample of 394 subjects that were included in the present study.

Image acquisition

Images were obtained in six different sites on 1.5 T systems from either General Electric (GE) or Siemens Medical Systems (Siemens) using a 3D T1-weighted spoiled gradient recalled (SPGR) echo sequence with the following parameters: TR = 22–25 ms, TE = 10–11 ms, excitation pulse = 30°, refocusing pulse = 180°, orientation: sagittal, field of view: AP = 256 mm; LR = 160–180 mm (whole-head coverage), and in-plane resolution = $1 \times 1 \times 1$ mm^3, where the maximum number of slices on the GE scanners was 124, and hence the slice thickness was 1.5 mm (Siemens: 1 mm).

Image processing

Preprocessing of the T1-weighted images was done using the SPM8 package (http://www.fil.ion.ucl.ac.uk/spm) and the VBM8 toolbox (http://dbm.neuro.uni-jena.de). All T1-weighted images were corrected for bias-field inhomogeneities, then spatially normalized and segmented into GM, WM, and cerebrospinal fluid (CSF) within the same generative model (Ashburner and Friston, 2005). The segmentation procedure was further extended by accounting for partial volume effects (Tohka et al., 2004), by applying adaptive maximum a posteriori estimations (Rajapakse et al., 1997), and by using a hidden Markov Random Field model (Cuadra et al., 2005), as described previously (Gaser, 2009).

In order to avoid introducing a systematic bias into the segmentation routine by using the standard adult reference data (Wilke et al., 2003), the Template-O-Matic toolbox (Wilke et al., 2008) was used within the unified segmentation framework to generate a sample-specific template. Thus, tissue segmentation does not rely on prior information maps, but solely on voxel intensity. This novel approach has already demonstrated robustness of the segmentation when handling MRI data from children (Altaye et al., 2008; Smith et al., 2011; Wilke et al., 2008). Since the removal of the prior tissue information makes the algorithm slightly less robust when confronted with lower quality input data (Wilke et al., 2008), all segmentation results were screened visually by one experienced rater (CG). The result was considered inadequate in 38 subjects.

Following the sequence proposed by Franke et al. (2010), the images were processed with affine registration and smoothed with 8 mm full-width-at-half-maximum (FWHM) smoothing kernels. Spatial resolution was set to 8 mm. Data reduction was performed by applying principal component analysis (PCA), utilizing the "Matlab Toolbox for Dimensionality Reduction" (http://ict.ewi.tudelft.nl/~lvandermaaten/Home.html).

Relevance vector regression (RVR)

Relevance vector machines (RVM) were introduced by Tipping (2000) as a Bayesian alternative to support vector machines (SVM) for obtaining sparse solutions to pattern recognition tasks. The main idea behind traditional SVMs is the transformation of training data from an input space into a high-dimensional space – the *feature space* – via a mapping function Φ (Bennett and Campbell, 2003; Schölkopf and Smola, 2002). For the purpose of classification, the hyperplane that best separates the groups is computed within this feature space, resulting in a nonlinear decision boundary within the input space. The best separating hyperplane is found by maximizing the margin between the two groups. The data points lying on the margin boundaries are called *support vectors* since only these are used to specify the optimal separating hyperplane. For the case of real-valued output functions (rather than just binary outputs as used in classification), the SV algorithm was generalized to a regression estimation (Bennett and Campbell, 2003; Schölkopf and Smola, 2002). In support vector regression (SVR), a function that fits as many data points as possible has to be found. Analogous to the margin in classification, the regression line is surrounded by a tube. Data points lying within that tube do not influence the course of the regression line. Data points lying on the edge or outside that tube are called *support vectors*.

Please cite this article as: Franke, K., et al., Brain maturation: Predicting individual *BrainAGE* in children and adolescents using structural MRI, NeuroImage (2012), http://dx.doi.org/10.1016/j.neuroimage.2012.08.001

In contrast to the support vectors in SVM, the *relevance vectors* in RVM represent the prototypical examples within the specified classification or regression task, instead of solely representing separating attributes. Furthermore severe overfitting associated with the maximum likelihood estimation of the model parameters was avoided by imposing an explicit zero-mean Gaussian prior (Ghosh and Mujumdar, 2008; Zheng et al., 2008). This prior is a characteristic feature of the RVM, and its use results in a vector of independent hyperparameters that reduces the data set (Faul and Tipping, 2002; Tipping, 2000; Tipping and Faul, 2003). Therefore, in most cases the number of relevance vectors is much smaller than the number of support vectors. In SVR, some additional parameters have to be determined or statistically optimized (e.g. with cross-validation loops) in order to control for model complexity and model fit. To control the behavior of the RVR, only the type of kernel has to be chosen. All other parameters are automatically estimated by the learning procedure itself. More details can be found elsewhere (Bishop, 2006; Schölkopf and Smola, 2002; Tipping, 2000).

Estimating BrainAGE

The *BrainAGE* framework utilizes RVR (Tipping, 2001) and was recently developed to estimate individual brain ages based on T1-weighted images (Franke et al., 2010). In general, the model is trained with preprocessed whole brain structural MRI data of the training sample. Subsequently, the brain age of a test subject can be estimated using the individual tissue-classified MRI data, aggregating the complex multidimensional aging pattern across the whole brain into one single value (Fig. 1A). The difference between the estimated and true chronological ages will reveal the individual *brain age gap estimation* (*BrainAGE*) score: the closer the estimated and the chronological ages are, the smaller is this value (Fig. 1B).

Within this study, the framework was applied using the linear combination of preprocessed GM and WM images. Since a leave-one-out approach is widely used in machine learning approaches and has been shown to provide a conservative estimate of a predictor's true accuracy (Dosenbach et al., 2010), model training and individual brain age estimation were done using leave-one-out-loops (i.e., the preprocessed GM and WM images of all subjects, except one, was used for training). Subsequently, the brain age of the left-out subject was estimated. PCA was performed on the training sample and the estimated parameters were subsequently applied to the test subjects. For training the model as well as for predicting individual brain ages, we utilized "The Spider" (http://www.kyb.mpg.de/bs/people/spider/main.html), a freely available toolbox running under MATLAB. For more detailed information please refer to Franke et al. (2010).

Statistical analysis

First, volumes of GM, WM, CSF, as well as total brain volume (TBV) were analyzed to explore the volume changes over development within this sample. To evaluate the accuracy of the age estimations, Pearson's linear correlation coefficient as well as the mean absolute error (MAE) between each subject's age and the age estimated by the regression model was established. Then, the brain maturation curve, including the 95% confidence interval for the prediction of brain age, was calculated using a regression model with a quadratic fit. To exclude unintended amplification effects while using coarse smoothing (i.e., 8 mm), training and testing of the *BrainAGE* framework were repeated with GM and WM images that were smoothed with a 4 mm FWHM smoothing kernel. Again, the accuracy of the new age estimations was evaluated using Pearson's linear correlation coefficient and MAE.

To assess the stability of *BrainAGE* estimation across different MRI scanner sites, age estimation was repeated for each of the six scanner sites separately. In other words, the *BrainAGE* model was trained with the data of five scanner sites and then applied to the data of the one left out in training. Pearson's linear correlation coefficient and the MAE between each subject's chronological age and the estimated age were calculated for each of the six scanner sites.

To exemplarily show the potential of the *BrainAGE* framework to differentiate between age groups, we divided the final 394 subjects into five age groups; each group spanned three consecutive years of age (Table 1). That is, preschool childhood (5–7 years), late childhood (8–10 years), early adolescence (11–13 years), middle adolescence (14–16 years), and late adolescence (17–19 years). The estimated brain ages as well as the volumes of GM, WM, CSF, and TBV were compared between these five age groups using analysis of variance (ANOVA). Post-hoc analyses (with Bonferroni adjustment to compensate for multiple comparisons) were conducted to explore significant group differences ($p<0.05$).

To further show the potential of the *BrainAGE* estimation framework with respect to modeling healthy brain maturation, receiver operating characteristics (ROC) for discriminating children (5–10 years) from adolescents (13–18 years) were computed for estimated brain age, GM volume, WM volume, CSF volume, and TBV, in order to demonstrate whether the brain age score adds information above and beyond that derived from tissue volumes alone. All statistical testing was performed using MATLAB.

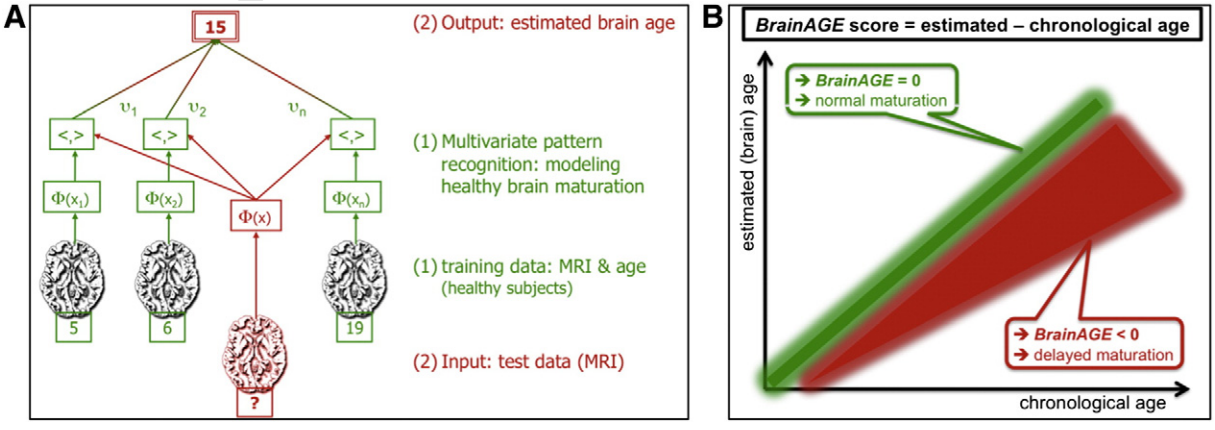

Fig. 1. The *BrainAGE* concept. A: The model of healthy brain aging is trained with preprocessed structural MRI data of a training sample (green). Subsequently, the individual brain ages of previously untested subjects are estimated, based on their MRI data (red). B: The difference between the estimated and chronological age results in the *BrainAGE* score. Consequently, negative *BrainAGE* scores indicate delayed brain maturation (red area). (For interpretation of the references to color in this figure legend, the reader is referred to the web version of this article.)
Panel A picture is modified from Schölkopf and Smola (2002).

Please cite this article as: Franke, K., et al., Brain maturation: Predicting individual *BrainAGE* in children and adolescents using structural MRI, NeuroImage (2012), http://dx.doi.org/10.1016/j.neuroimage.2012.08.001

Table 1
Subject demographics and between-group differences (NIH normal brain development sample).

	Preschool childhood	Late childhood	Early adolescence	Middle adolescence	Late adolescence	F	p
Age range (years)	5–7	8–10	11–13	14–16	17–19	–	–
Number of subjects	126	97	77	60	34	–	–
Males/females	68/58	54/43	38/39	29/31	18/16	–	–
GM volume (ml)	745.9	747.7	738.5	718.7	680.0	8.5	<0.001
WM volume (ml)	469.5	490.4	514.3	538.5	537.1	18.4	<0.001
CSF volume (ml)	145.5	157.3	161.5	177.3	188.9	28.3	<0.001
TBV (ml)	1360.9	1395.4	1414.3	1434.5	1406.0	4.6	<0.01
Estimated brain age (years)	6.99	9.61	12.28	15.09	16.32	439.9	<0.001

Exemplary application of the BrainAGE framework to clinical data

To exemplarily show the potential of the *BrainAGE* framework to provide clinically relevant information, the age of adolescents born very preterm and with extremely low birth weight (i.e., before the beginning of the 33rd week of gestation and weighing <1500 g) was estimated. Prematurity is known to be a considerable risk factor for later developmental disabilities (Allen, 2008) and was chosen here as a model for an early interference with normal brain development. The MR data was acquired on a 1.5 T Siemens Avanto Scanner (Siemens Medizintechnik, Erlangen, Germany), using a 12-channel head coil. A T1-weighted 3D-data set (MPRAGE, TR = 1300 ms, TE = 2.92 ms, 176 contiguous slices with an in-plane matrix of 256×256, yielding a voxel size of $1\times1\times1$ mm^3) was acquired. Parallel imaging was not used.

The age estimation model was trained with all 394 subjects from the NIH sample. Subsequently, the brain ages of the preterm-born adolescents were estimated. As described above, for each subject in the training set as well as in the test set the linear combination of preprocessed GM and WM images was used. PCA was performed on the training sample and the estimated parameters were subsequently applied to the test sample. The resulting *BrainAGE* scores were compared between those subjects who were born before the end of the 27th week of gestation (GA<27; n = 10) versus those who were born after the end of the 29th week of gestation (GA>29; n = 15), using Student's *t*-test. To evaluate the accuracy of the age estimations in both groups, Pearson's linear correlation coefficient between the chronological and estimated ages and MAE (after adjusting the estimated ages to a zero mean) were calculated. Detailed characteristics of both groups can be found in Table 2.

Results

Within our test sample of 394 healthy children and adolescents, aged 5–18 years (mean age = 10.7 years; SD = 3.9 years), the developmental changes with respect to GM, WM, CSF, and TB volumes are comparable to those reported in the literature (Giedd et al., 1999; Giedd et al., 2009; Groeschel et al., 2010; Silk and Wood, 2011). More specifically, while the trajectory of GM volume exhibits an inverted U-shape, WM volume increases steadily with age (Fig. 2).

The correlation between the estimated age and true age was r = 0.93 (p<0.001). Thus, 87% of variance between the chronological age and the age estimated based on structural MRI was explained. The MAE was 1.1 years. As shown in Fig. 3, the 95% confidence interval for the prediction of brain age (±2.6 years) was stable across the entire age range. To exclude unintended amplification effects while using coarse smoothing, training and testing of the *BrainAGE* framework were repeated with images that were smoothed with a 4 mm FWHM smoothing kernel. However, prediction accuracy remained stable (r = 0.93; MAE = 1.2 years).

Since multivariate pattern recognition techniques such as RVR are able to use the whole pattern in the brain image as well as interregional dependencies, the multidimensional maturation pattern used for brain age estimation was widespread across the whole brain. For an exemplary illustration, the most important features (i.e., the importance of voxel locations for regression with age) that were used by the RVR are shown in Fig. S1 for GM and Fig. S2 for WM.

When the *BrainAGE* model was trained with the data of five MRI scanner sites and then applied to the one left out in training, estimation accuracy proved to remain stable across all scanner sites. The correlations between the chronological and estimated ages ranged between r = 0.90 and r = 0.95 (p<0.001). The MAEs ranged between 1.1 and 1.3 years (Table 3).

When exemplarily comparing the five predefined age groups (i.e., preschool childhood, late childhood, early adolescence, middle adolescence, and late adolescence), the estimated brain ages differed between the age groups (F = 439.9; p<0.001; Table 1), with post-hoc t-tests resulting in differences (p<0.05) between all five age groups (Fig. 4). For volumes of GM, WM, CSF, and TBV the ANOVA also resulted in significant differences (Table 1), but post-hoc t-tests did not result in differences between all of the five age groups.

Based on these encouraging results, we conducted an additional ANOVA to explore group differences with respect to estimated brain ages between neighboring ages (i.e., 5-years old vs. 6-years old, etc.). Again, the results showed differences in estimated brain ages between neighboring age groups (F = 208.9; p<0.001; Fig. S3), suggesting the existence of specific, and therefore identifiable, age-dependent brain maturation patterns.

Binary classification of individuals as either children (aged 5–10 years) or adolescents (aged 13–18 years), based on their estimated brain age, was 97% accurate (sensitivity = 98%, specificity = 96%). The area under the ROC curve (AUC), which is also known as the c-statistic or c-index, shows the quality of the classification, with 1.0 indicating a perfect discrimination and 0.5 indicating a result obtained by chance only. As demonstrated in Fig. 5, AUC was 0.996 when discriminating children and adolescents using the estimated brain ages. In contrast, when using CSF volume to classify individuals as either children or adolescents, the accuracy rate was 73% and AUC was 0.78. Other parameters were even less sensitive (i.e., accuracy: GM volume = 63%; WM volume = 72%; TBV = 59%; AUC: GM volume = 0.65; WM volume = 0.74; TBV = 0.61).

Finally, the *BrainAGE* framework was exemplarily applied to structural MRI data of preterm-born adolescents, aged between 12 and 16 years at the time of the MR scan. The *BrainAGE* scores differed significantly (p<0.01; df = 23) between group GA<27 (i.e., subjects who were born before the end of the 27th week of gestation) and group GA>29 (i.e., subjects who were born after the end of the 29th week of gestation) and revealed the following means (SD): GA<27 = −1.96

Table 2
Subject demographics (preterm-born adolescents).

	Gestational age<27 weeks	Gestational age>29 weeks
Number of subjects	10	15
Mean (SD) age at gestation (weeks)	25.4 (0.8)	30.3 (0.7)
Mean (SD) age at MR scan (years)	14.3 (1.4)	14.7 (1.5)

Please cite this article as: Franke, K., et al., Brain maturation: Predicting individual *BrainAGE* in children and adolescents using structural MRI, NeuroImage (2012), http://dx.doi.org/10.1016/j.neuroimage.2012.08.001

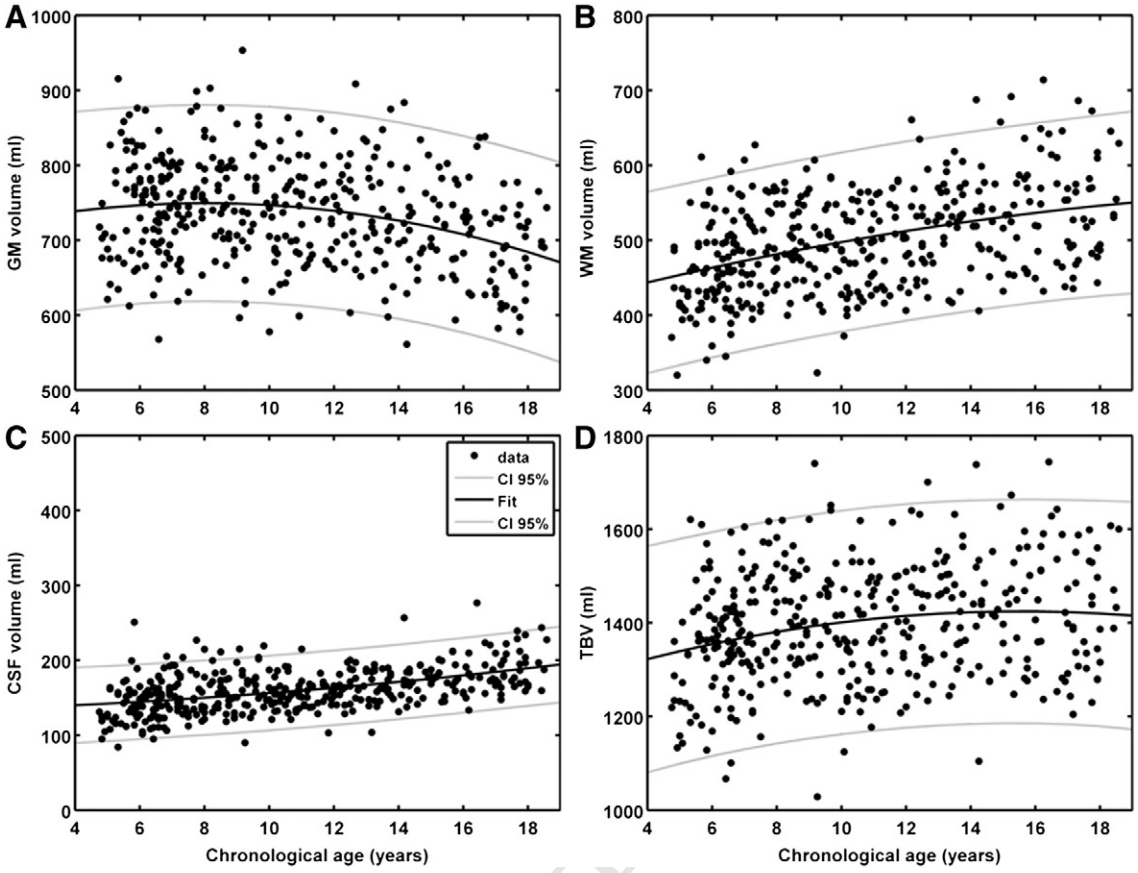

Fig. 2. Brain tissue and brain volume trajectories across development. The change of individual tissue volumes across development with 95% confidence intervals (light lines) of the quadratic fits (bold lines) for GM (A), WM (B), CSF (C), and TBV (D).

(0.68) years, GA > 29 = −0.40 (1.50) years (Fig. 6). Although the mean difference in the gestation age between both groups was only 5 weeks, these results show a systematically and dramatically lower *BrainAGE* score in the group of adolescents who were born extremely preterm, implying delayed brain maturation.

In both groups, prediction accuracy was high resulting in correlation coefficients between the estimated and chronological ages of $r = 0.89$ ($p < 0.001$) and $r = 0.75$ ($p < 0.01$) for the groups GA < 27 and GA > 29, respectively. After adjusting the estimated ages to a zero mean, MAE would result in 0.5 years and 1.1 years, respectively. Again the *BrainAGE* framework proved to provide reliable estimations even with entirely new data that differed from the training data by scanner and by scanning parameters.

Discussion

The present study provides a sensitive and easy-to-use reference curve for structural brain maturation during childhood and adolescence. The novel *BrainAGE* concept adopted here combines the complex multidimensional maturation pattern across the whole brain into one single value. Using structural MRI data of 394 healthy subjects (aged 5 to 18 years) acquired on six different scanners, we predicted a maturation curve that accounted for 87% sample variance. Furthermore, a strong stability of the estimated brain ages across different MRI scanner sites was demonstrated. The framework showed exemplary predictive value, classifying individuals as children (age range 5–10 years) or adolescents (age range 13–18 years) with 97% accuracy. Moreover, the predicted brain age demonstrated its potential to differentiate between all age groups (i.e., preschool childhood, late childhood, early adolescence, middle adolescence, and late adolescence) and even between neighboring ages. Finally, the *BrainAGE* framework exemplarily showed its potential to provide clinically relevant information. With a mean difference in *BrainAGE* scores of −1.6 years between the early preterms and the late preterms, the adolescents who were born extremely preterm showed clear signs of delayed brain maturation.

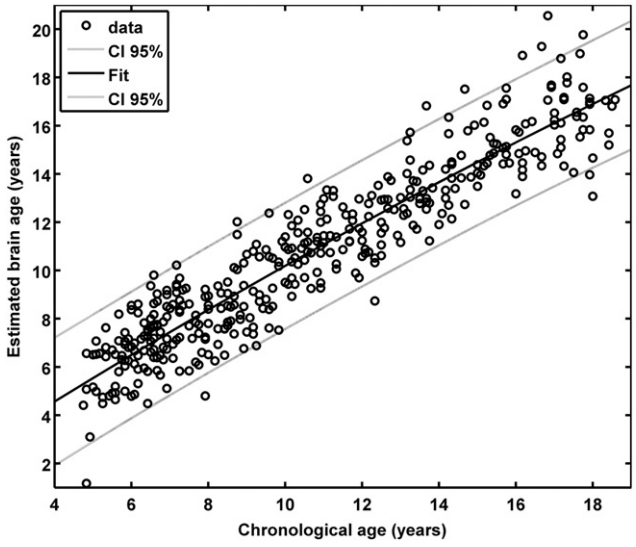

Fig. 3. Estimated brain maturation using *BrainAGE*. Individual structural brain age based on anatomical T1-images of 394 healthy subjects (aged 5–18 years). Chronological age is shown on the x-axis and the estimated brain age on the y-axis. The 95% confidence interval of the quadratic fit is stable across the age range (±2.6 years).

Please cite this article as: Franke, K., et al., Brain maturation: Predicting individual *BrainAGE* in children and adolescents using structural MRI, NeuroImage (2012), http://dx.doi.org/10.1016/j.neuroimage.2012.08.001

Table 3
Stability of *BrainAGE* estimation across different MRI scanner sites. The model was trained with the data of five scanner sites and then applied to the one left out in training (test sample).

	Scanner site (as test sample)					
	1	2	3	4	5	6
Scanner	GE Genesis Signa	GE Genesis Signa	GE Genesis Signa	GE Genesis Signa	Siemens Sonata	Siemens Magneton Vision
Number of subjects	53	76	71	75	48	70
Age range (years)	4.8–17.8	4.8–18.5	5.1–18.6	4.8–18.0	5.0–17.8	6.2–18.4
Mean (SD) age (years)	10.7 (4.0)	10.5 (3.8)	11.8 (4.1)	10.4 (4.0)	9.8 (3.8)	10.8 (3.4)
r	0.95	0.92	0.92	0.93	0.91	0.90
MAE (years)	1.1	1.2	1.3	1.2	1.3	1.2

Several structural MRI studies of brain maturation have already shown the age-dependent development of a variety of brain measures in children and adolescents. Although the human brain has reached 95% of its maximum size by the age of six, the cortical and subcortical components of the brain still change dramatically during childhood and adolescence (Lenroot and Giedd, 2006). While GM volumes follow regionally-specific inverted U-shaped developmental curves, with volumes peaking at different times across the different lobes, WM volume changes were thought to be more linear and less variant across regions (Giedd et al., 1999; Lenroot and Giedd, 2006). Recently, Lebel and Beaulieu (2011) showed significant nonlinear development trajectories also for WM, with maturation being complete by late adolescence for projection and commissural tracts, but association tracts maturing well beyond adolescence. Furthermore, GM and WM development during childhood and adolescence appeared to reveal regionally specific, age-dependent variations (Wilke and Holland, 2003). Taken together, brain maturation is not only a very complex multidimensional but also a highly variable process. In the light of the multitude of these brain changes, it is remarkable that the confidence interval does not change substantially as a function of age, underlining the potential of the approach to correctly capture the multidimensional characteristics of the different maturational processes occurring in this age range.

In their groundbreaking study, Dosenbach et al. (2010) already emphasized the need of maturation curves for pediatric brain development to aid in the early detection of neurodevelopmental disorders. For example, childhood-onset schizophrenia was found to show a similar but abnormally accelerated pattern as seen during normal brain maturation (i.e., accelerated GM loss in a characteristic back-to-front (parieto-frontal–temporal) direction during adolescent years (Gogtay et al., 2004; Gogtay and Thompson, 2010; Thompson et al., 2001)).

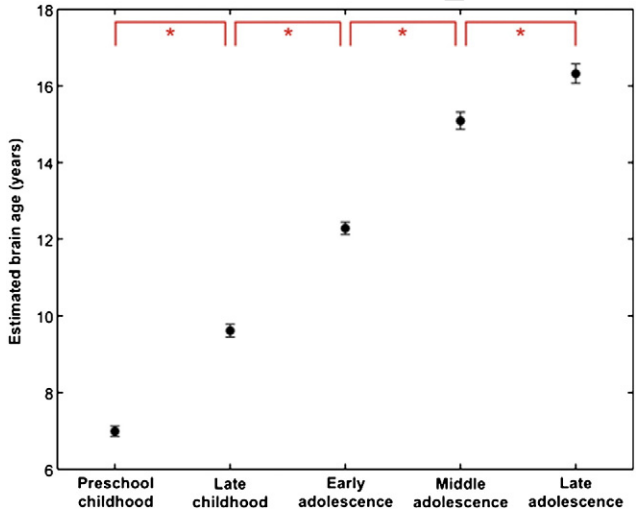

Fig. 4. Age group differentiation using *BrainAGE*. Mean of estimated brain ages by predefined age groups. Error bars depict the standard error of the mean (SEM). Post-hoc t-tests resulted in significant differences between all five age groups ($p<0.05$; red lines). (For interpretation of the references to color in this figure legend, the reader is referred to the web version of this article.)

Interestingly though, these accelerated GM deficits are not likely to be the result of WM overgrowth because WM growth itself was shown to be decelerated by about 2% in patients with childhood-onset schizophrenia compared to healthy controls (Gogtay et al., 2008; Gogtay and Thompson, 2010; Paus et al., 2001).

Using only one structural MR image per subject, the maturation curve predicted by the *BrainAGE* framework accounted for 87% of the sample variance and proved its potential to recognize delayed brain maturation in a clinical sample. Hence, our novel *BrainAGE* framework is a valuable complement to Dosenbach's maturation index of functional connectivity that accounted for 55% sample variance (Dosenbach et al., 2010). It is conceivable that the combination of structural and functional image data might achieve an even higher accuracy, although the required multidimensional dataset from each subject would constitute a clear drawback. Importantly, structural MRI is already the imaging modality of choice in most centers and especially with children. Moreover, structural imaging avoids the possible bias due to individual differences in alertness and vigilance, a severely confounding factor when using functional MRI (Van Dijk et al., 2012). Luckily, given the novel results of the *BrainAGE* algorithm, the aforementioned need for multidimensional data is no longer pressing.

An additional challenge when establishing a clinically valuable reference curve for structural brain maturation is developing an algorithm, which allows combining MRI data from different scanners. When applying the estimation procedures to MRI data from a scanner, which was not included during the training of the algorithm, the *BrainAGE* framework demonstrated strong stability of the estimated brain age ($r=0.90–0.95$). Even with entirely new data that differed from the training data not only by scanner but also by scanning parameters, the *BrainAGE* framework proved to provide reliable estimates plus clinically valuable information. Thus, our results are in line with those of Klöppel et al. (2008), indicating that the effect of the scanner parameters is sufficiently different from that of the aging process and that linear RVR generalizes well across different scanners.

However, given the nature of data included in this study, our conclusions are limited to MRI data obtained with 1.5 T field strengths. As already shown previously (Franke et al., 2010), numerous variables have the potential to influence the accuracy of age prediction, such as the number of subjects constituting the training sample (which added most on variability), various parameters pertaining to data acquisition (e.g., field strength, scanning sequence) and data preprocessing (e.g., registration, smoothing), as well as the chosen approach to reduce data dimensionality (e.g. PCA). Therefore, these aforementioned aspects need to be carefully controlled in future studies. Future work will further explore the influences of varying parameters in data acquisition on prediction accuracy.

In order to facilitate usability in a clinical routine, the algorithm should work fast and fully automatic. As already indicated in Franke et al. (2010), a fairly rapid preprocessing of the MRI data can be achieved by performing affine registration with a large smoothing kernel (e.g., 8 mm). Even in estimating the brain maturation in children and adolescents a coarse spatial resolution (e.g., 8 mm) can be used without losing estimation accuracy. Unlike approaches that make use

Please cite this article as: Franke, K., et al., Brain maturation: Predicting individual *BrainAGE* in children and adolescents using structural MRI, NeuroImage (2012), http://dx.doi.org/10.1016/j.neuroimage.2012.08.001

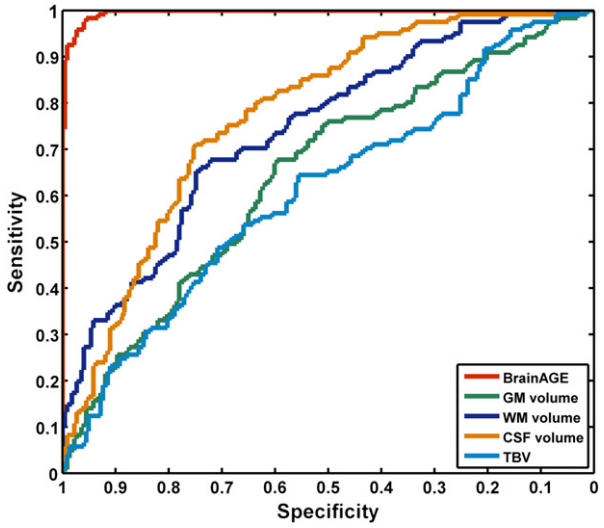

Fig. 5. ROC curves of subject classification using *BrainAGE*. ROC curves of individual subject classification as either children (aged 5–10 years) or adolescents (aged 13–18 years) based on estimated brain age (red; AUC = 0.99), GM volume (dark blue; AUC = 0.65), WM volume (light blue; AUC = 0.74), and TBV (green; AUC = 0.61). (For interpretation of the references to color in this figure legend, the reader is referred to the web version of this article.)

of specified regional information, multivariate pattern recognition techniques, such as RVR, are fully automatic and make use of the whole pattern in the brain image (see also Klöppel et al., 2008). Additionally, inter-regional dependencies are taken into account (Bishop, 2006; Schölkopf and Smola, 2002), such as the widespread microstructural changes in WM, which were recently found to be associated with corresponding age-related changes in cortical GM regions in adolescents (Giorgio et al., 2010; Giorgio et al., 2008). When modeling brain maturation within the *BrainAGE* approach, the multidimensional maturation pattern used for brain age estimation was also found to be widespread across the whole brain, including increases as well as decreases.

Directly quantifying the degree of acceleration or deceleration of brain maturation in terms of years, adopting our novel *BrainAGE* concept will allow a wide range of analyses and predictions to aid in the early detection of neurodevelopmental disorders on an individual level. With significantly lower *BrainAGE* scores in adolescents who were born preterm, the present study additionally demonstrated the potential of the *BrainAGE* framework to recognize neurodevelopmental delays. Besides, the potential to provide clinically relevant information was already shown previously by reporting a positive deviation between estimated and chronological age of about 10 years in patients with Alzheimer's disease, indicating accelerated brain atrophy (Franke et al., 2010). In the future, applying the *BrainAGE* framework to clinically relevant samples as well as tracking the performance of our age estimation model with follow-up MRI data may further elucidate the prognostic value of the *BrainAGE* score.

However, it should be noted, that the *BrainAGE* approach was implemented to model "normal" structural brain maturation or brain aging (Franke et al., 2010). Therefore, and in this stage of model development, the application to clinical samples is only recommended if the underlying disease is likely a result of overall deceleration or acceleration of brain maturation or brain aging, such as observed in subjects with developmental delays (Harbord et al., 1990; McLaughlin et al., 2010; Ramenghi et al., 2011; Verbruggen et al., 2009), schizophrenia (Kirkpatrick et al., 2008), or Alzheimer's disease (Cao et al., 2010; Driscoll et al., 2009; Dukart et al., 2011; Jones et al., 2011; Saetre et al., 2011; Spulber et al., 2010). Future work will extend the current approach to allow identifying significant regional deviations from the expected age-specific pattern in order to provide region-specific information as a basis for further clinical applications.

To summarize, we demonstrated the potential of the *BrainAGE* framework to reliably predict brain maturity in children and adolescents and to provide a clinically sensitive as well as easy-to-use reference curve of healthy brain maturation. We have also shown that this method can be used across different scanners (see also Franke et al., 2010), which is an important prerequisite for use in clinical routines. Given that the *BrainAGE* framework is validated as well as fast and easy to use, this method holds great potential for application in daily clinical routine, especially since brain imaging has become part of the standard diagnostic work-up for many developmental neuropsychiatric disorders. Nevertheless, combining different imaging techniques holds the potential to further improve existing analysis streams (e.g. Dosenbach et al., 2010; Franke et al., 2010), and combining structural and functional connectivity imaging may reveal a valuable biomarker in the future to guide early detection in the prodromal phase of diseases.

Supplementary data to this article can be found online at http://dx.doi.org/10.1016/j.neuroimage.2012.08.001.

Disclosure

The authors report no conflict of interest.

Acknowledgment

We are grateful to Dr. Alissa Winkler for her comments on the manuscript. We would also like to thank Till-Karsten Hauser (University Hospital Tübingen) as well as Karen Lidzba, Andrea Bevot, and Rangmar Goelz (University Children's Hospital Tübingen), for their help with patient recruitment and characterization. This work was supported by BMBF grant 01EV0709.

This manuscript reflects the views of the authors and may not reflect the opinions or views of the Brain Development Cooperative Group Investigators or the NIH. A listing of the participating sites in the NIH MRI study of normal brain development and a complete listing of the study investigators can be found at the website of the data coordinating center at https://nihpd.crbs.ucsd.edu/nihpd/info/participating_centers.html.

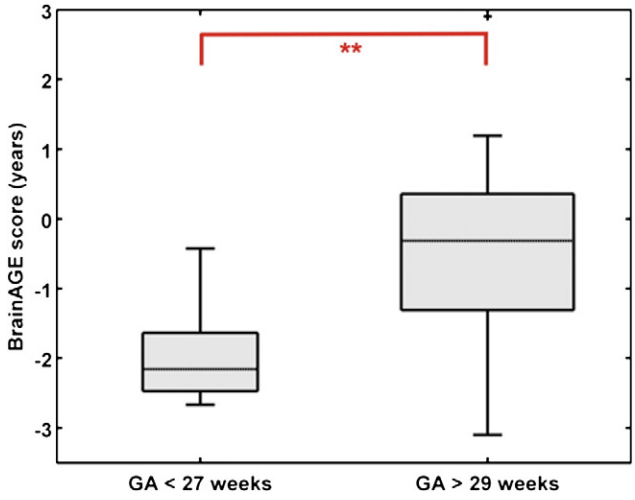

Fig. 6. *BrainAGE* scores in preterm-born adolescents. Shown are box plots with *BrainAGE* scores (in years) for those adolescents who were born before the end of the 27th week of gestation (mean = −2.0) vs. those who were born after the end of the 29th week of gestation (mean = −0.4). The gray boxes contain the values between the 25th and 75th percentiles of the samples, including the median (dashed line). Lines extending above and below each box symbolize data within 1.5 times the interquartile range (outliers are displayed with a +). The width of the boxes depends on the sample size. Student's *t*-test resulted in a significant difference between both groups ($p<0.01$; red lines). (For interpretation of the references to color in this figure legend, the reader is referred to the web version of this article.)

References

Allen, M.C., 2008. Neurodevelopmental outcomes of preterm infants. Curr. Opin. Neurol. 21, 123–128.

Altaye, M., Holland, S.K., Wilke, M., Gaser, C., 2008. Infant brain probability templates for MRI segmentation and normalization. NeuroImage 43, 721–730.

Ashburner, J., Friston, K.J., 2000. Voxel-based morphometry—the methods. NeuroImage 11, 805–821.

Ashburner, J., Friston, K.J., 2005. Unified segmentation. NeuroImage 26, 839–851.

Bennett, K.P., Campbell, C., 2003. Support vector machines: hype or hallelujah? SIGKDD Explor. 2, 1–13.

Bishop, C.M., 2006. Pattern Recognition and Machine Learning. Springer, New York, NY.

Cao, K., Chen-Plotkin, A.S., Plotkin, J.B., Wang, L.S., 2010. Age-correlated gene expression in normal and neurodegenerative human brain tissues. PLoS One 5.

Cuadra, M.B., Cammoun, L., Butz, T., Cuisenaire, O., Thiran, J.P., 2005. Comparison and validation of tissue modelization and statistical classification methods in T1-weighted MR brain images. IEEE Trans. Med. Imaging 24, 1548–1565.

Dosenbach, N.U., Nardos, B., Cohen, A.L., Fair, D.A., Power, J.D., Church, J.A., Nelson, S.M., Wig, G.S., Vogel, A.C., Lessov-Schlaggar, C.N., Barnes, K.A., Dubis, J.W., Feczko, E., Coalson, R.S., Pruett Jr., J.R., Barch, D.M., Petersen, S.E., Schlaggar, B.L., 2010. Prediction of individual brain maturity using fMRI. Science 329, 1358–1361.

Driscoll, I., Davatzikos, C., An, Y., Wu, X., Shen, D., Kraut, M., Resnick, S.M., 2009. Longitudinal pattern of regional brain volume change differentiates normal aging from MCI. Neurology 72, 1906–1913.

Dukart, J., Schroeter, M.L., Mueller, K., 2011. Age correction in dementia—matching to a healthy brain. PLoS One 6, e22193.

Evans, A.C., 2006. The NIH MRI study of normal brain development. NeuroImage 30, 184–202.

Faul, A., Tipping, M.E., 2002. Analysis of sparse Bayesian learning. In: Dietterich, T.G., Becker, S., Ghahramani, Z. (Eds.), Advances in Neural Information Processing Systems, 14. MIT Press, pp. 383–389.

Franke, K., Ziegler, G., Klöppel, S., Gaser, C., Initiative, t.A.s.D.N., 2010. Estimating the age of healthy subjects from T1-weighted MRI scans using kernel methods: exploring the influence of various parameters. NeuroImage 50, 883–892.

Gaser, C., 2009. Partial volume segmentation with adaptive maximum a posteriori (MAP) approach. NeuroImage 47, S121.

Ghosh, S., Mujumdar, P.P., 2008. Statistical downscaling of GCM simulations to streamflow using relevance vector machine. Adv. Water Resour. 31, 132–146.

Giedd, J.N., Snell, J.W., Lange, N., Rajapakse, J.C., Casey, B.J., Kozuch, P.L., Vaituzis, A.C., Vauss, Y.C., Hamburger, S.D., Kaysen, D., Rapoport, J.L., 1996. Quantitative magnetic resonance imaging of human brain development: ages 4–18. Cereb. Cortex 6, 551–560.

Giedd, J.N., Blumenthal, J., Jeffries, N.O., Castellanos, F.X., Liu, H., Zijdenbos, A., Paus, T., Evans, A.C., Rapoport, J.L., 1999. Brain development during childhood and adolescence: a longitudinal MRI study. Nat. Neurosci. 2, 861–863.

Giedd, J.N., Lalonde, F.M., Celano, M.J., White, S.L., Wallace, G.L., Lee, N.R., Lenroot, R.K., 2009. Anatomical brain magnetic resonance imaging of typically developing children and adolescents. J. Am. Acad. Child Adolesc. Psychiatry 48, 465–470.

Giorgio, A., Watkins, K.E., Douaud, G., James, A.C., James, S., De Stefano, N., Matthews, P.M., Smith, S.M., Johansen-Berg, H., 2008. Changes in white matter microstructure during adolescence. NeuroImage 39, 52–61.

Giorgio, A., Watkins, K.E., Chadwick, M., James, S., Winmill, L., Douaud, G., De Stefano, N., Matthews, P.M., Smith, S.M., Johansen-Berg, H., James, A.C., 2010. Longitudinal changes in grey and white matter during adolescence. NeuroImage 49, 94–103.

Gogtay, N., Thompson, P.M., 2010. Mapping gray matter development: implications for typical development and vulnerability to psychopathology. Brain Cogn. 72, 6–15.

Gogtay, N., Giedd, J.N., Lusk, L., Hayashi, K.M., Greenstein, D., Vaituzis, A.C., Nugent 3rd, T.F., Herman, D.H., Clasen, L.S., Toga, A.W., Rapoport, J.L., Thompson, P.M., 2004. Dynamic mapping of human cortical development during childhood through early adulthood. Proc. Natl. Acad. Sci. U. S. A. 101, 8174–8179.

Gogtay, N., Lu, A., Leow, A.D., Klunder, A.D., Lee, A.D., Chavez, A., Greenstein, D., Giedd, J.N., Toga, A.W., Rapoport, J.L., Thompson, P.M., 2008. Three-dimensional brain growth abnormalities in childhood-onset schizophrenia visualized by using tensor-based morphometry. Proc. Natl. Acad. Sci. U. S. A. 105, 15979–15984.

Groeschel, S., Vollmer, B., King, M.D., Connelly, A., 2010. Developmental changes in cerebral grey and white matter volume from infancy to adulthood. Int. J. Dev. Neurosci. 28, 481–489.

Harbord, M.G., Finn, J.P., Hall-Craggs, M.A., Robb, S.A., Kendall, B.E., Boyd, S.G., 1990. Myelination patterns on magnetic resonance of children with developmental delay. Dev. Med. Child Neurol. 32, 295–303.

Jones, D.T., Machulda, M.M., Vemuri, P., McDade, E.M., Zeng, G., Senjem, M.L., Gunter, J.L., Przybelski, S.A., Avula, R.T., Knopman, D.S., Boeve, B.F., Petersen, R.C., Jack Jr., C.R., 2011. Age-related changes in the default mode network are more advanced in Alzheimer disease. Neurology 77, 1524–1531.

Kirkpatrick, B., Messias, E., Harvey, P.D., Fernandez-Egea, E., Bowie, C.R., 2008. Is schizophrenia a syndrome of accelerated aging? Schizophr. Bull. 34, 1024–1032.

Klöppel, S., Stonnington, C.M., Chu, C., Draganski, B., Scahill, R.I., Rohrer, J.D., Fox, N.C., Jack Jr., C.R., Ashburner, J., Frackowiak, R.S., 2008. Automatic classification of MR scans in Alzheimer's disease. Brain 131, 681–689.

Lebel, C., Beaulieu, C., 2011. Longitudinal development of human brain wiring continues from childhood into adulthood. J. Neurosci. 31, 10937–10947.

Lenroot, R.K., Giedd, J.N., 2006. Brain development in children and adolescents: insights from anatomical magnetic resonance imaging. Neurosci. Biobehav. Rev. 30, 718–729.

May, A., 2011. Experience-dependent structural plasticity in the adult human brain. Trends Cogn. Sci. 15, 475–482.

McLaughlin, K.A., Fox, N.A., Zeanah, C.H., Sheridan, M.A., Marshall, P., Nelson, C.A., 2010. Delayed maturation in brain electrical activity partially explains the association between early environmental deprivation and symptoms of attention-deficit/hyperactivity disorder. Biol. Psychiatry 68, 329–336.

Paus, T., Collins, D.L., Evans, A.C., Leonard, G., Pike, B., Zijdenbos, A., 2001. Maturation of white matter in the human brain: a review of magnetic resonance studies. Brain Res. Bull. 54, 255–266.

Paus, T., Keshavan, M., Giedd, J.N., 2008. Why do many psychiatric disorders emerge during adolescence? Nat. Rev. Neurosci. 9, 947–957.

Rajapakse, J.C., Giedd, J.N., Rapoport, J.L., 1997. Statistical approach to segmentation of single-channel cerebral MR images. IEEE Trans. Med. Imaging 16, 176–186.

Ramenghi, L.A., Martinelli, A., De Carli, A., Brusati, V., Mandia, L., Fumagalli, M., Triulzi, F., Mosca, F., Cetin, I., 2011. Cerebral maturation in IUGR and appropriate for gestational age preterm babies. Reprod. Sci. 18, 469–475.

Saetre, P., Jazin, E., Emilsson, L., 2011. Age-related changes in gene expression are accelerated in Alzheimer's disease. Synapse 65, 971–974.

Schölkopf, B., Smola, A., 2002. Learning with Kernels: Support Vector Machines, Regularization, Optimization, and Beyond. MIT Press, Cambridge, Mass.

Silk, T.J., Wood, A.G., 2011. Lessons about neurodevelopment from anatomical magnetic resonance imaging. J. Dev. Behav. Pediatr. 32, 158–168.

Smith, K.M., Mecoli, M.D., Altaye, M., Komlos, M., Maitra, R., Eaton, K.P., Egelhoff, J.C., Holland, S.K., 2011. Morphometric differences in the Heschl's gyrus of hearing impaired and normal hearing infants. Cereb. Cortex 21, 991–998.

Spulber, G., Niskanen, E., MacDonald, S., Smilovici, O., Chen, K., Reiman, E.M., Jauhiainen, A.M., Hallikainen, M., Tervo, S., Wahlund, L.O., Vanninen, R., Kivipelto, M., Soininen, H., 2010. Whole brain atrophy rate predicts progression from MCI to Alzheimer's disease. Neurobiol. Aging 31, 1601–1605.

Thompson, P.M., Vidal, C., Giedd, J.N., Gochman, P., Blumenthal, J., Nicolson, R., Toga, A.W., Rapoport, J.L., 2001. Mapping adolescent brain change reveals dynamic wave of accelerated gray matter loss in very early-onset schizophrenia. Proc. Natl. Acad. Sci. U. S. A. 98, 11650–11655.

Tipping, M., 2000. The relevance vector machine. In: Solla, S.A., Leen, T.K., Müller, K.-R. (Eds.), Advances in Neural Information Processing Systems, 12. MIT Press, pp. 652–658.

Tipping, M.E., 2001. Sparse Bayesian learning and the relevance vector machine. J. Mach. Learn. Res. 1, 211–244.

Tipping, M.E., Faul, A.C., 2003. Fast marginal likelihood maximisation for sparse Bayesian models. In: Bishop, C.M., Frey, B.J. (Eds.), Proceedings of the Ninth International Workshop on Artificial Intelligence and Statistics, Key West, FL.

Tohka, J., Zijdenbos, A., Evans, A., 2004. Fast and robust parameter estimation for statistical partial volume models in brain MRI. NeuroImage 23, 84–97.

Van Dijk, K.R., Sabuncu, M.R., Buckner, R.L., 2012. The influence of head motion on intrinsic functional connectivity MRI. NeuroImage 59, 431–438.

Verbruggen, K.T., Meiners, L.C., Sijens, P.E., Lunsing, R.J., van Spronsen, F.J., Brouwer, O.F., 2009. Magnetic resonance imaging and proton magnetic resonance spectroscopy of the brain in the diagnostic evaluation of developmental delay. Eur. J. Paediatr. Neurol. 13, 181–190.

Wilke, M., Holland, S.K., 2003. Variability of gray and white matter during normal development: a voxel-based MRI analysis. Neuroreport 14, 1887–1890.

Wilke, M., Schmithorst, V.J., Holland, S.K., 2003. Normative pediatric brain data for spatial normalization and segmentation differs from standard adult data. Magn. Reson. Med. 50, 749–757.

Wilke, M., Holland, S.K., Altaye, M., Gaser, C., 2008. Template-O-Matic: a toolbox for creating customized pediatric templates. NeuroImage 41, 903–913.

Yuan, W., Altaye, M., Ret, J., Schmithorst, V., Byars, A.W., Plante, E., Holland, S.K., 2009. Quantification of head motion in children during various fMRI language tasks. Hum. Brain Mapp. 30, 1481–1489.

Zheng, Y.-T., Neo, S.-Y., Chua, T.-S., Tian, Q., 2008. Probabilistic optimized ranking for multimedia semantic concept detection via RVM. Proceedings of the 2008 international conference on Content-based image and video retrieval. ACM, Niagara Falls, Canada, pp. 161–168.

Please cite this article as: Franke, K., et al., Brain maturation: Predicting individual *BrainAGE* in children and adolescents using structural MRI, NeuroImage (2012), http://dx.doi.org/10.1016/j.neuroimage.2012.08.001